J|A|C|S
ARTICLES
Published on Web 08/02/2007

"Open Rather than Closed" Malonate Methano-Fullerene Derivatives. The Formation of Methanofulleroid Adducts of $Y_3N@C_{80}$

Olena Lukoyanova,[†] Claudia M. Cardona,[†] José Rivera,[†] Leyda Z. Lugo-Morales,[†] Christopher J. Chancellor,[‡] Marilyn M. Olmstead,[‡] Antonio Rodríguez-Fortea,[§] Josep M. Poblet,*[,§] Alan L. Balch,[‡] and Luis Echegoyen*[,†]

Contribution from the Department of Chemistry, Clemson University, Clemson, South Carolina 29634, Department of Chemistry, University of California, Davis, One Shields Avenue, Davis, California 95616, and Departament de Química Física i Inorgànica, Universitat Rovira i Virgili, c/Marcel·lí Domingo, s/n, Campus Sescelades, 43007 Tarragona, Spain

Received March 12, 2007; E-mail: albalch@ucdavis.edu; josepmaria.poblet@urv.cat; luis@clemson.edu

Abstract: Cycloaddition of bromomalonates to $Y_3N@C_{80}$ unexpectedly gave rise to fulleroid derivatives with unusually high stability. Complete characterization of these derivatives is described including X-ray crystallography, ^{1}H NMR, ^{13}C NMR, HMQC, UV−visible, HPLC, MALDI-MS, and electrochemistry. Density functional theory calculations are also presented, which provide a rationale for the formation of the fulleroid and reveal the underlying thermodynamic basis for their stability.

Introduction

Recent investigations in the field of endohedral metallofullerenes (EMFs) have provided new insights into the properties of these fascinating molecules.[1−19] Many of these reports describe methods of exohedral functionalization for EMFs, isolation of the derivatives, and subsequent studies of their properties. Most commonly, the functionalization of EMFs was accomplished using various addition reactions, similar to those developed earlier for empty fullerenes. However, the chemical reactivity of endohedral fullerenes has proven to be very different from that of their empty cage counterparts and has shown, perhaps not surprisingly, a dependency on the nature of the encapsulated species. Furthermore, with the readily abundant I_h $M_3N@C_{80}$ EMFs, addition can occur at either a [5,6] or a [6,6] ring junction, whereas addition reactions for C_{60} generally occur at the localized double bonds at [6,6] junctions. The chemistry of EMFs is a reasonably new area of research that has intensified in the past few years from the advent of newly developed methodology to produce these materials in gram-scale quantities.

EMFs have considerable potential for applications that utilize the magnetic, spectroscopic, and nuclear properties of the metal ions encapsulated inside. Thus, EMFs containing paramagnetic Gd(III) have been shown to be effective relaxation agents for magnetic resonance imaging (MRI).[20−22] EMFs also have promise as hosts for radioactive atoms for use in nuclear medicine.[23−25] To customize the biological behavior of these EMFs, it will be necessary to functionalize them with external appendages that can confer suitable solubilities and reactivities.

Recent work has focused on exploring the chemistry and characterizing the electrochemical behavior of a particular family of EMFs, the trimetallic nitride endohedral metallofullerenes, which are also known as Trimetasphere carbon nanomaterials (TMSs).[26] The most abundant of these endohedrals consist of

[†] Clemson University.
[‡] University of California.
[§] Universitat Rovira i Virgili.

(1) Yamada, M.; et al. *J. Am. Chem. Soc.* **2006**, *128*, 1402−1403.
(2) Wakahara, T.; et al. *J. Am. Chem. Soc.* **2006**, *128*, 9919−9925.
(3) Shu, C.-Y.; Gan, L.-H.; Wang, C.-R.; Pei, X.-l.; Han, H.-b. *Carbon* **2006**, *44*, 496−500.
(4) Feng, L.; et al. *Chem.-Eur. J.* **2006**, *12*, 5578−5586.
(5) Feng, L.; et al. *J. Am. Chem. Soc.* **2006**, *128*, 5990−5991.
(6) Cardona, C. M.; Elliott, B.; Echegoyen, L. *J. Am. Chem. Soc.* **2006**, *128*, 6580−6485.
(7) Cai, T.; et al. *J. Am. Chem. Soc.* **2006**, 6486−6492.
(8) Campanera, J. M.; Bo, C.; Poblet, J. M. *J. Org. Chem.* **2006**, *71*, 46−54.
(9) Echegoyen, L.; Chancellor, C. J.; Cardona, C. M.; Elliott, B.; Rivera, J.; Olmstead, M. M.; Balch, A. L. *Chem. Commun.* **2006**, 2653−2655.
(10) Cardona, C. M.; Kitaygorodskiy, A.; Echegoyen, L. *J. Am. Chem. Soc.* **2005**, *127*, 10448−10453.
(11) Yamada, M.; et al. *J. Am. Chem. Soc.* **2005**, *127*, 14570−14571.
(12) Yamada, M.; et al. *J. Phys. Chem. B* **2005**, *109*, 6049−6051.
(13) Stevenson, S.; Stephen, R. R.; Amos, T. M.; Cadorette, V. R.; Reid, J. E.; Phillips, J. P. *J. Am. Chem. Soc.* **2005**, *127*, 12776−12777.
(14) Kareev, I. E.; Lebedkin, S. F.; Bubnov, V. P.; Yagubskii, E. B.; Ioffe, I. N.; Khavrel, P. A.; Kuvychko, I. V.; Strauss, S. H.; Boltalina, O. V. *Angew. Chem., Int. Ed.* **2005**, *44*, 1846−1849.
(15) Iiduka, Y.; et al. *J. Am. Chem. Soc.* **2005**, *127*, 9956−9957.
(16) Ge, Z. X.; Duchamp, J. C.; Cai, T.; Gibson, H. W.; Dorn, H. C. *J. Am. Chem. Soc.* **2005**, *127*, 16292−16298.
(17) Feng, L.; et al. *J. Am. Chem. Soc.* **2005**, *127*, 17136−17137.
(18) Cardona, C. M.; Kitaygorodskiy, A.; Ortiz, A.; Herranz, M. A.; Echegoyen, L. *J. Org. Chem.* **2005**, *70*, 5092−5097.
(19) Cai, T.; Ge, Z. X.; Iezzi, E. B.; Glass, T. E.; Harich, K.; Gibson, H. W.; Dorn, H. C. *Chem. Commun.* **2005**, 3594−3596.
(20) Mikawa, M.; Kato, H.; Okumura, M.; Narazaki, M.; Kanazawa, Y.; Miwa, N.; Shinohara, H. *Bioconjugate Chem.* **2001**, *12*, 510−514.
(21) Bolskar, R. D.; Benedetto, A. F.; Husebo, L. O.; Price, R. E.; Jackson, E. F.; Wallace, S.; Wilson, L. J.; Alford, J. M. *J. Am. Chem. Soc.* **2003**, *125*, 5471−5478.
(22) Fatouros, P. P.; et al. *Radiology* **2006**, *240*, 756−764.
(23) Wilson, L. J.; Cagle, D. W.; Thrash, T. P.; Kennel, S. J.; Mirzadeh, S.; Alford, J. M.; Ehrhardt, G. J. *Coord. Chem. Rev.* **1999**, *192*, 199−207.
(24) Da Ros, T.; Prato, M. *Chem. Commun.* **1999**, 663−669.
(25) Li, Q. N.; Xiu, Y.; Zhang, X. D.; Liu, R. L.; Du, Q. Q.; Shun, X. G.; Chen, S. L.; Li, W. X. *Nucl. Med. Biol.* **2002**, *29*, 707−710.
(26) Stevenson, S.; et al. *Nature* **1999**, *401*, 55−57.

C_{80} cages with icosahedral symmetry (I_h). These cages encapsulate trimetallic nitride clusters, M_3N, such as Sc_3N, Y_3N, Er_3N, Lu_3N, Gd_3N, etc. The first TMS adduct, a Diels−Alder cycloadduct of $Sc_3N@C_{80}$ at a [5,6] junction, was reported by Dorn, Balch, and co-workers in 2002.[27,28] It was not until 2005 that other types of derivatives were reported.[10,18,19] Interestingly, the 1,3-dipolar cycloaddition of an *N*-ethyl azomethine ylide displayed selectivity depending on the metal cluster.[10,18] When the cluster was Sc_3N, the only product recovered was the adduct at a [5,6] double bond, just like the case of the Diels−Alder derivative. On the other hand, the 1,3-dipolar cycloaddition occurred at a [6,6] double bond junction for $Y_3N@C_{80}$ and $Er_3N@C_{80}$. These [6,6] monoadducts proved to be the kinetic product, and they underwent rearrangement to the thermodynamically more stable [5,6] monoadducts upon heating.[6] Recently,[7] both the [6,6] and the [5,6] pyrrolidine monoadducts of $Sc_3N@C_{80}$ were isolated when an *N*-trityl azomethine ylide was employed instead of *N*-methyl or *N*-ethyl analogues. In related work, Akasaka and co-workers have explored the *N*-trityl pyrrolidine adduct of $La_2@C_{80}$.[1] These experimental results, as well as recent computational studies by Poblet and Echegoyen,[29] seem to indicate that the pyrrolidine adduct is kinetically favored at the [6,6] sites and a thermal rearrangement, facilitated by the heteroatom on the pyrrolidine ring, gives rise to the [5,6] monoadduct that is energetically preferred. The rate of this rearrangement not only depends on the internal cluster, but on the pyrrolidine addend itself. Echegoyen et al. have also shown that these species have fascinating electrochemical properties.[6] The pristine species $M_3N@C_{80}$ (M = Sc, Y, Er) as well as their [6,6] monoadducts exhibit electrochemically irreversible reductive behavior, while their [5,6] monoadducts display reversible behavior using cyclic voltammetry. Additionally, retro-cycloaddition of the [5,6] *N*-ethyl pyrrolidine derivatives of $Sc_3N@C_{80}$ and $Y_3N@C_{80}$ occurs under both thermal and oxidative electrochemical conditions. This process can be used as a strategy to extract I_h $M_3N@C_{80}$ from mixtures containing the D_{5h} isomer.[30,31]

Interestingly, the [2+1] cycloaddition of bromodiethylmalonate (the Bingel−Hirsch reaction) in the presence of the nonnucleophilic base 1,8-diazabicyclo[5.4.0]-undec-7-ene (DBU) produced extremely stable derivatives with $Y_3N@C_{80}$ (**1**, $Y_3N@C_{80}-C(CO_2Et)_2$) and $Er_3N@C_{80}$,[6] while $Sc_3N@C_{80}$ did not react under the same experimental conditions.[10] ^{1}H NMR and electrochemical characterization seemed to indicate that the cycloaddition occurred at a [6,6] double bond site, and the assumption was that these were "closed" bis(ethoxycarbonyl)-methano derivatives.

Results

Synthesis and Stability of Bingel−Hirsch Adducts. Samples of **1**, $Y_3N@C_{80}-C(CO_2Et)_2$ (as reported earlier),[10] and **2**, $Y_3N@C_{80}-C(CO_2CH_2Ph)_2$, were obtained by the addition of the appropriate bromomalonate to $Y_3N@C_{80}$ in the presence DBU, as outlined for **2** in Scheme 1.

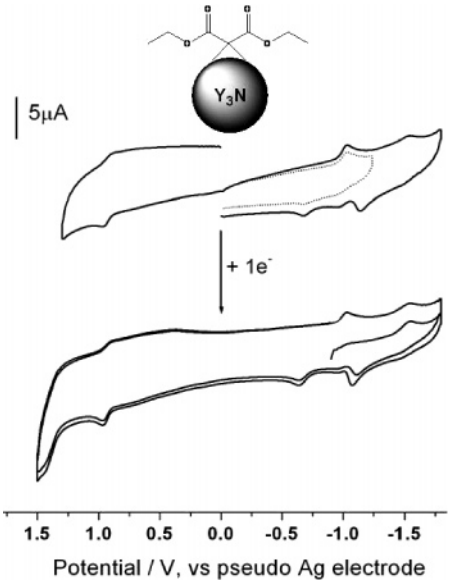

Figure 1. CPE experiment (0.05 M $TBAPF_6$ in *o*-dichlorobenzene) of **1** (1 mg), $Y_3N@C_{80}-C(CO_2Et)_2$. The upper trace shows the CV (100 mV/s) for the sample before electrolysis, while the lower trace shows the CV taken under the same conditions after **1** was converted to its monoanionic state at −1.25 V (vs Ag pseudo reference electrode). After reoxidation to its neutral state, no changes in its electrochemical behavior were noted.

Scheme 1. Synthesis of **2**, $Y_3N@C_{80}-C(CO_2CH_2Ph)_2$[a]

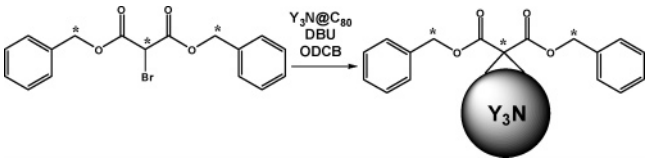

[a] The asterisks show the positions that were labeled with ^{13}C.

These adducts are remarkably stable. In an attempt to obtain the corresponding [5,6] regioisomer, a sample of **1** was heated for 21 h at 180 °C without detecting any observable changes.

Because bis(alkoxycarbonyl)methano fullerenes are known to undergo facile reductive retro-cyclopropanation reaction,[32] we assumed that it would be possible to remove the methano addend by chemical or electrochemical reductive means. However, exhaustive reduction by controlled potential electrolysis (CPE) resulted in no changes in the electrochemical behavior, as studied by cyclic voltammetry (CV), and in the NMR spectrum of the compound. Figure 1 shows a particular CPE experiment where **1** was reduced to its monoanionic state at −1.3 V (vs Ag pseudo reference electrode). Reoxidation of this material resulted in the complete recovery of the starting material. In a similar fashion, exposure of **1** to sodium metal in THF under vacuum resulted in fragmentation of the malonate groups, but the methano carbon remained attached to the $Y_3N@C_{80}$ cage, as observed by MALDI-MS (Figure 2). To the best of our knowledge, this is the first bis(alkoxycarbonyl)-methano fullerene that possesses exceptional stability toward reductive retro-cycloaddition reaction.

So far, attempts to crystallize **1** to characterize its structure by X-ray crystallography were not successful. However, crystals

(27) Iezzi, E. B.; Duchamp, J. C.; Harich, K.; Glass, T. E.; Lee, H. M.; Olmstead, M. M.; Balch, A. L.; Dorn, H. C. *J. Am. Chem. Soc.* **2002**, *124*, 524−525.
(28) Lee, H. M.; Olmstead, M. M.; Iezzi, E.; Duchamp, J. C.; Dorn, H. C.; Balch, A. L. *J. Am. Chem. Soc.* **2002**, *124*, 3494−3495.
(29) Rodriguez-Fortea, A.; Campanera, J. M.; Cardona, C. M.; Echegoyen, L.; Poblet, J. M. *Angew. Chem., Int. Ed.* **2006**, *45*, 8176−8180.
(30) Martin, N.; Altable, M.; Filippone, S.; Martin-Domenech, A.; Echegoyen, L.; Cardona, C. M. *Angew. Chem., Int. Ed.* **2006**, *45*, 110−114.
(31) Lukoyanova, O.; Cardona, C. M.; Altable, M.; Filippone, S.; Domenech, A. M.; Martin, N.; Echegoyen, L. *Angew. Chem., Int. Ed.* **2006**, *45*, 7430−7433.
(32) Herranz, M. A.; Diederich, F.; Echegoyen, L. *Eur. J. Org. Chem.* **2004**, 2299−2316.

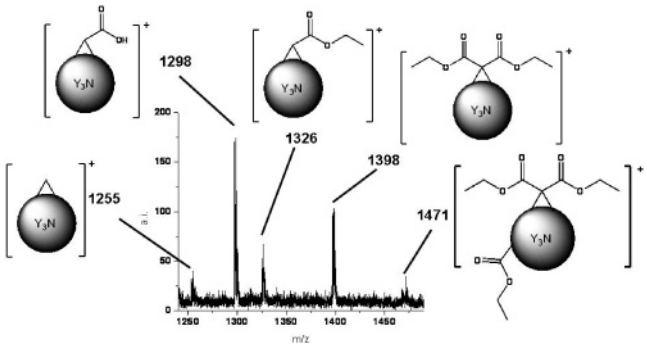

Figure 2. MALDI spectrum of a sample of **1**, $Y_3N@C_{80}-C(CO_2Et)_2$, after chemical reduction with sodium metal in THF. No traces of the pristine $Y_3N@C_{80}$ were detected (see Supporting Information).

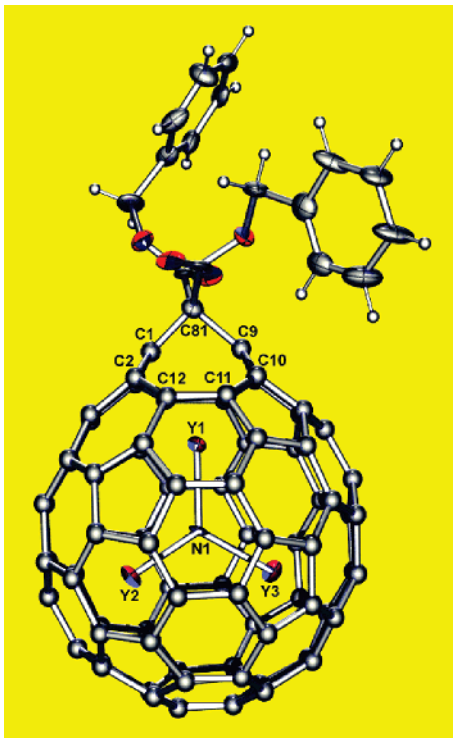

Figure 3. A drawing of the Bingel adduct $Y_3N@C_{80}-C(CO_2CH_2Ph)_2$ with 50% thermal contours for those atoms refined anisotropically and uniform circles for the carbon atoms of the fullerene. Only one orientation of the fullerene cage is shown, and only the major orientation of the Y_3N group is shown. Interatomic distances: Y1−N, 2.066(8); Y2−N, 2.042 (9); Y3−N, 2.098 (9) Å.

of **2**, $Y_3N@C_{80}-C(CO_2CH_2Ph)_2$, were obtained. Unexpectedly, the X-ray structure revealed that this adduct was a fulleroid of $Y_3N@C_{80}$, where the C−C bond at the site of addition on the fullerene is broken, or open.

Characterization by Single-Crystal X-ray Diffraction. Black crystals of $Y_3N@C_{80}-C(CO_2CH_2Ph)_2\cdot0.5C_6H_6\cdot0.5CHCl_3$ used to obtain the crystallographic data were obtained by gradual evaporation of a solution of **2** in chloroform with layers of benzene and acetone placed above. The drawing of the adduct shown in Figure 3 reveals that the addition has occurred at a [6,6] ring junction as is generally the case for the formation of methano adducts of fullerenes via the Bingel−Hirsch reaction.

It is clear that a C−C bond at a [6,6] ring junction of the original $Y_3N@C_{80}$ has broken upon formation of the derivative, although there is disorder in the cage orientation for another portion of this endohedral (vide infra). Figure 3 was drawn to

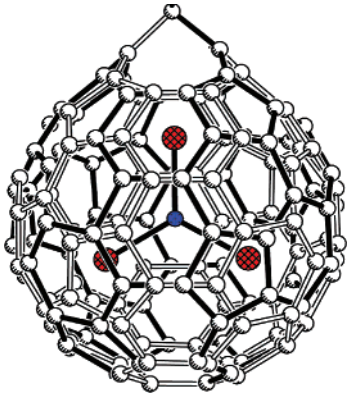

Figure 4. A drawing showing the two orientations of the fullerene cage and the major (0.70 occupancy) orientation of the Y_3N unit in the Bingel adduct $Y_3N@C_{80}-C(CO_2CH_2Ph)_2$.

emphasize the elongation of the C1−C9 separation. Whereas the average C−C bond at a [6,6] ring junction in I_h $Sc_3N@C_{80}$ has a length of 1.421(18) Å,[28] the C1−C9 distances in the Bingel−Hirsch adduct $Y_3N@C_{80}-C(CO_2CH_2Ph)_2$ are opened to 2.30(3) for one orientation of the cage and 2.28(4) Å in the other orientation. Thus, in this case a fulleroid rather than a methanofullerene has formed.

Generally, methano adduct formation on empty cage fullerenes like C_{60} results in the formation of methanofullerenes with a [6,6] closed structure.[33] There are two exceptions that have been crystallographically characterized. A homofullerene, $C_{70}-CCl_2$, produced by reaction of C_{70} with $PhHgCCl_2Br$, has been reported.[34] In this material, adduct formation occurs at a [5,6] ring junction involving the C7−C8 bond, and the critical C7−C8 distances in the adduct are 2.136(6) and 2.139(6) Å in the two crystallographically independent molecules in the unit cell. In the case of $La@C_{82}$, a modified carbene addition of an adamantylidene moiety produces a fulleroid, $La@C_{82}-(Ad)$, at a [6,6] ring junction as studied by Akasaka and co-workers (vide infra).[37] In this case, the opened C−C separation is 2.097 Å. It has also been reported that the two isolated isomers of $C_{60}-CF_2$ have open structures with the major isomer involving addition to a [6,6] site while the minor isomer involves addition to a [5,6] site.[35]

The crystal structure of **2** shows some disorder in the position of the cage carbon atoms. In the orientation of the cage shown in Figure 3, there is a five-membered ring containing C1 on the left side of the site of addition and a six-membered ring containing C9 on the right side. The second orientation is produced by interchanging the locations of these five- and six-membered rings as well as of the rest of the carbon cage. This process produces minimal changes in the external shape of the cage.

Figure 4 shows how these two orientations are related. In this drawing, the orientation corresponding to that in Figure 3 is shown with open lines connecting the atoms, while the second

(33) Hirsch, A. *The Chemistry of the Fullerenes*; G. Thieme Verlag: Stuttgart; New York, 1994.
(34) Kiely, A. F.; Haddon, R. C.; Meier, M. S.; Selegue, J. P.; Brock, C. P.; Patrick, B. O.; Wang, G. W.; Chen, Y. S. *J. Am. Chem. Soc.* **1999**, *121*, 7971−7972.
(35) Pimenova, A. S.; Kozlov, A. A.; Goryunkov, A. A.; Markov, V. Y.; Khavrel, P. A.; Avdoshenko, S. M.; Ioffe, I. N.; Sakharov, S. G.; Troyanov, S. I. Sidorov, L. N. *Chem. Commun.* **2007**, 374−376.
(36) Miller, G. P.; Tetreau, M. C.; Olmstead, M. M.; Lord, P. A.; Balch, A. L. *Chem. Commun.* **2001**, 1758−1759.
(37) Maeda, Y.; et al. *J. Am. Chem. Soc.* **2004**, *126*, 6858−6859.

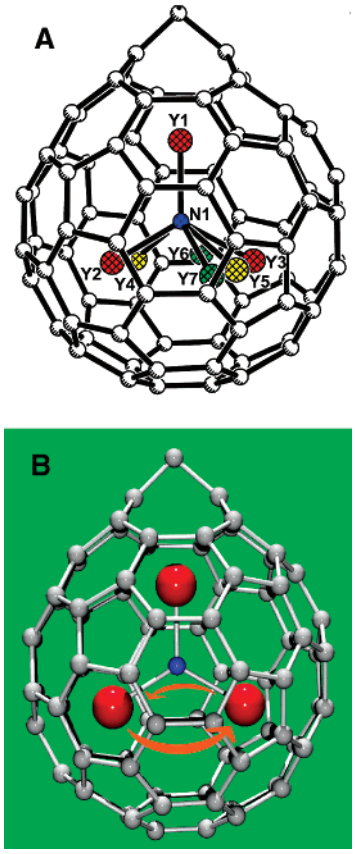

Figure 5. (A) A drawing showing the three orientations of the Y_3N units in the Bingel adduct $Y_3N@C_{80}-C(CO_2CH_2Ph)_2$. Yttrium ions in the major, planar site (0.70 occupancy) are colored red. The Y ions colored yellow combine with fully occupied Y1 to form a second planar Y_3N group with 0.21 fractional occupancy. The Y ions colored green combine with Y1 to form a Y_3N group with 0.09 occupancy. (B) A drawing showing the proposed spinning of the Y_3N group about the N1−Y1 axis.

orientation is shown with solid lines connecting the atoms. Such orientational disorder is common for fullerenes functionalized in this fashion. For example, the [6,6] isomers of the 1,3-dipolar cycloadducts of *N*-trityl azomethine ylide, $Sc_3N@C_{80}-(CH_2)_2NCPh_3$ and $La_2@C_{80}-(CH_2)_2NCPh_3$,[1,7] show similar disorder, as do other empty cage fullerene adducts.[36]

The Y_3N group in $Y_3N@C_{80}-C(CO_2CH_2Ph)_2$ is also disordered. The major orientation with 0.70 occupancy is shown in Figures 3 and 4. The Y_3N unit is planar in this orientation with the sum of the three N−Y−N angles equal to 359.9°. A second orientation with 0.21 occupancy also utilizes Y1, which is at full occupancy, and two other yttrium atom sites (Y4 and Y5) as shown in Figure 5A.

This orientation of the Y_3N group is also planar with the sum of the angles equal to 359.7°. The final orientation with 0.09 fractional occupancy again utilizes Y1 this time in combination with Y6 and Y7. This site has a pyramidalized Y_3N group with the sum of the three Y−N−Y angles being 348.2°. However, this value may be misleading because the site has low occupancy and only one nitrogen atom position at the center of the endohedral has been defined. It is important to note that the Y_3N group in the [5,6] pyrrolidine adduct, $Y_3N@C_{80}-(CH_2)_2NEt$, is slightly pyramidalized with the sum of the three Y−N−Y angles being 358.8°.[9] The flattening of the Y_3N group in the Bingel−Hirsch adduct $Y_3N@C_{80}-C(CO_2CH_2Ph)_2$ may

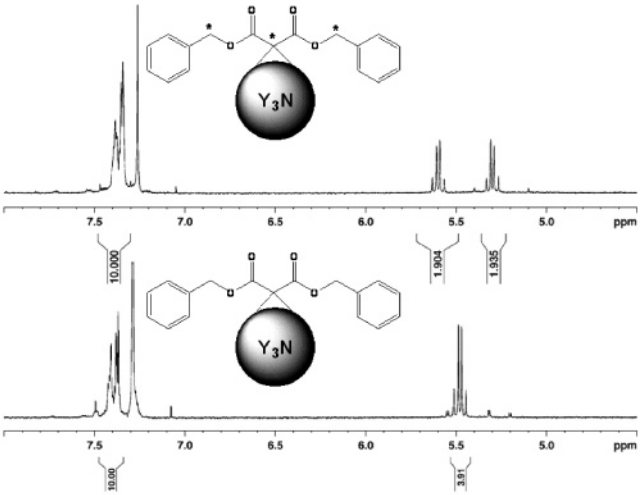

Figure 6. Comparison of the ^1H NMR spectra of top, ^{13}C-labeled **2**, $Y_3N@C_{80}-C(CO_2CH_2Ph)_2$; and bottom, unlabeled **2**.

well be the result of the additional space provided inside the cage by the opening of the C1−C9 bond in the adduct.

It is significant to note that Y1 in $Y_3N@C_{80}-C(CO_2CH_2Ph)_2$ is positioned near the site of the cleaved bond formerly between C1 and C9. There are several Y−C contacts in this region with distances in the 2.47−2.57 Å range. The other yttrium atoms are situated further from the neighboring carbon atoms. A similar situation involving metal ion location was observed in the case of the modified carbene-type adduct, $La@C_{82}$−adamantylidene.[37] Here again the metal atom resides in the site nearest the place where one of the C−C bonds at a [6,6] ring junction has been opened as its X-ray crystal structure has shown. The presence of alternate positions for two of the three yttrium ions in $Y_3N@C_{80}-C(CO_2CH_2Ph)_2$ suggests that at higher temperatures than the 90 K used for the structure determination, the Y_3N group is free to spin as a top about the N−Y1 axis as shown in Figure 5B.

Spectroscopic Studies. Because only limited amounts of $Y_3N@C_{80}$ were available, we decided to use ^{13}C-labeled bis-(benzyloxycarbonyl) bromomalonate to obtain the Bingel−Hirsch adduct **2** and facilitate the examination of the NMR spectra. As shown in Scheme 1, labels were introduced at the central carbon atom and at the two methylene carbon atoms. Spectra of both labeled and unlabeled samples were obtained and compared.

The ^1H NMR spectrum of the unlabeled product shown in Figure 6 clearly shows that the methylene protons are prochiral and give rise to an AB doublet of doublets. In the ^{13}C-labeled product, these are further split into two symmetrical resonances due to the coupling with the ^{13}C methylene-carbon atom.

The HMQC and the ^{13}C NMR spectra of the labeled adduct clearly display two resonances corresponding to the two types of ^{13}C-labeled carbons: the methylene carbons at 69.54 and the methano carbon at 61.46 ppm (Figure 7).

The fact that only one methylene resonance was present confirms that addition occurred at a [6,6]-site. The chemical shift of the methano carbon atom is similar to that of Akasaka's derivative, the anion of $La@C_{82}C(COOC_2H_5)_2$, which shows a corresponding resonance at 65.74 ppm.[4]

The UV−visible spectra of **2** and its precursor, $Y_3N@C_{80}$, are similar as shown in Figure 8. This similarity indicates that

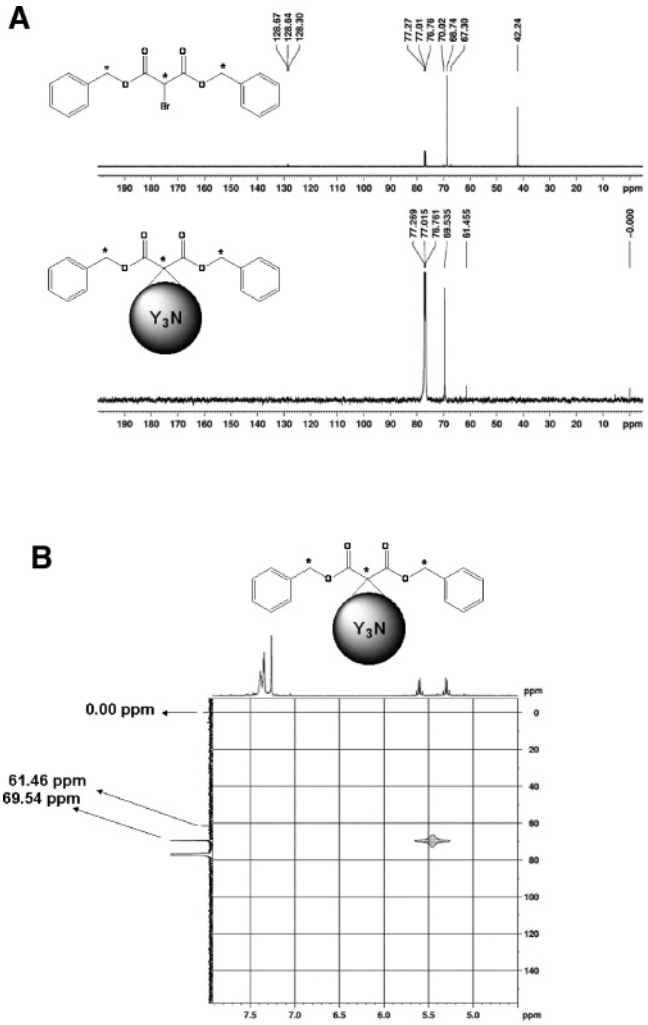

Figure 7. (A) ^{13}C NMR spectra of ^{13}C-labeled bis(benzyloxycarbonyl) bromomalonate (top) and that of the adduct **2**, $Y_3N@C_{80}-C(CO_2CH_2Ph)_2$ (bottom) in $CDCl_3$. (B) HMQC spectrum of ^{13}C-labeled **2**, $Y_3N@C_{80}-C(CO_2CH_2Ph)_2$.

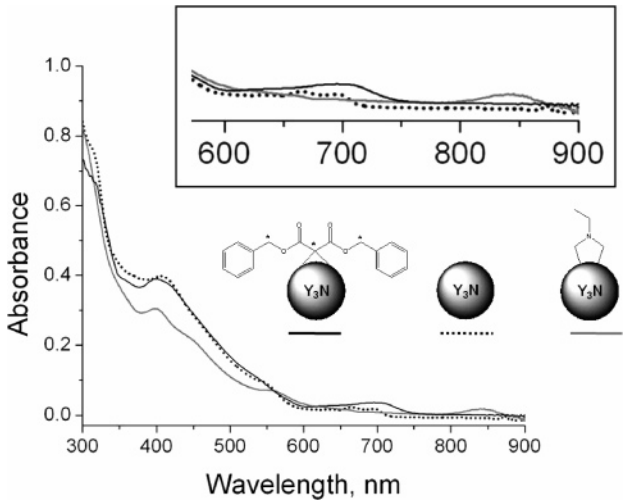

Figure 8. UV−visible spectra of **2**, $Y_3N@C_{80}-C(CO_2CH_2Ph)_2$ (33 μM, solid black line), $Y_3N@C_{80}$ (38 μM, dotted line), and $Y_3N@C_{80}-(CH_2)_2$-NEt (28 μM, gray line). The inset shows an expansion of the 600−800 nm region.

the number of radial p orbitals in the adduct is the same as in the precursor and that the adduct is a fulleroid. For comparison, we have included the spectrum of the *N*-ethyl [5,6]-pyrrolidino

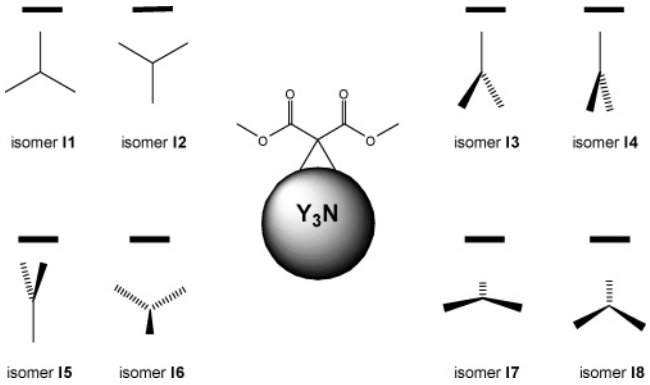

Figure 9. Representations of the relative position of the TNT unit (shown as a Y-shaped figure) with respect to the position of external functionalization (indicated by a bar) for the different isomers computed in this work.

Table 1. Bond Energies[a] (in kcal mol^{-1}) for the Different Product Isomers of the Bingel−Hirsch Reaction of $Y_3N@C_{80}$[b]

isomer	[5,6]		[6,6]	
I1	−73.0	(4.8)	−77.7	(0.0)
I2	−60.4	(17.4)	−51.6	(26.2)
I3	−74.4	(3.4)	−77.3	(0.5)
I4	−73.8	(3.9)	−75.6	(2.2)
I5	−45.7	(32.1)	−46.3	(31.5)
I6	−57.0	(20.7)	−52.3	(25.4)
I7	−48.5	(29.3)	−50.4	(27.3)
I8	−49.5	(28.2)	−49.1	(28.6)

[a] The bond energies (BE) are defined in the following way: BE = E[product] − E[$Y_3N@C_{80}$] − E[$C(COOCH_3)_2$]. [b] Relative energies (in kcal mol^{-1}) with respect to the lowest energy minimum in parentheses. The bond energies for the products of the Bingel−Hirsch reaction to the [5,6] and [6,6] bonds of C_{80} are −63.9 and −57.9 kcal/mol, respectively.

derivative of $Y_3N@C_{80}$, which has been characterized by X-ray crystallography.[9] The latter displays major spectral differences that cannot be attributed to the addend itself such as the large absorption at 842 nm, which is absent from the spectra of the adduct **2** and of $Y_3N@C_{80}$.

Computational Analysis of the Stability of the Metallofulleroid. As already mentioned, the functionalization of endohedral metallofullerenes based on the I_h isomer of C_{80} can lead to two different regioisomers depending on the addition site, the [5,6] ring junction or the [6,6] ring junction. Moreover, for each of these regioisomers, there are different possible orientations of the encapsulated metal cluster inside the carbon cage. For TMSs, the trimetallic nitride template (TNT) unit can easily rotate in underivatized $M_3N@C_{80}$ (M = Sc, Y) compounds.[38] However, the rotation inside the functionalized fullerene is more hindered for the products of the Diels−Alder and the 1,3-dipolar cycloaddition reactions and produces different, "orientational" isomers.[8,29,38] We have analyzed some of these representative isomers for the case of the Bingel−Hirsch reaction (Figure 9).

Our computational model is $Y_3N@C_{80}-C(CO_2CH_3)_2$ in which the ethyl and benzyl groups are substituted by the simpler methyl group. From Table 1, we observe fairly high bond energies between the carbon cage and the $C(CO_2CH_3)_2$ group, indicating the strength of the formed bonds, a fact that is in good agreement with the exceptional stability of the product. The isomers with one of the Y atoms pointing toward the methano group show the lowest energies. In particular, the [6,6]

(38) Campanera, J. M.; Bo, C.; Olmstead, M. M.; Balch, A. L.; Poblet, J. M. *J. Phys. Chem. A* **2002**, *106*, 12356−12364.

Table 2. Selected Distances (in Å) of the [6,6]-Methano Derivative of $Y_3N@C_{80}$ As Obtained from X-ray Diffraction As Compared to DFT Results for [6,6] Isomer **I1**

distances[a]	X-ray	DFT
Y1−N	2.066	2.081
Y2−N/Y3−N[c]	2.070	2.072
C1···C9[b]	2.29	2.277
C1−C81/C9−C81[c]	1.533	1.503
Y1−C1/Y1−C9[c]	2.528	2.549

[a] See Figure 3 for atom labeling. [b] Average value of the distance for two different open structures. [c] Average value of the two different distances.

isomer **I1** is the most stable structure, in excellent agreement with the experimental data. The energy of the other orientational isomers is much higher (>17 kcal mol^{-1}). Consequently, rotation of the TNT unit inside the functionalized fullerene is partially hindered as has been found to be the case for other types of derivatives, and the most favorable conformations are those with a Y atom pointing to the external group, in good agreement with X-ray data. Some bonding interactions between the Y atom and the C atoms that have been functionalized seem to be present. A detailed analysis of the molecular orbitals for isomers **I1**, **I3**, and **I4**, as well as for the related system with La_2 instead of the TNT unit, shows that the Y···C bonding interaction is not described by a single molecular orbital, but by many of them. In these circumstances, methods based on the analysis of the electron density distribution and its derivatives become more illustrative.[39,40] The Laplacian of electron density distribution (Figure S7 in Supporting Information) for the [6,6] isomer **I1** shows that interaction between the fullerene cage and Y_3N can be described as ionic. The presence of some accumulations of the electron density in carbon atoms 1 and 9 oriented toward the yttrium ion (Y1) suggests some coordinative interaction that transfers electron density from the anionic cage toward the metal via the substituted carbon atoms (see Supporting Information for more details). This coordinative interaction fixes the position of Y1 but Y2 and Y3 may rotate freely as shown in Figure 5 and confirmed by the almost degenerate energies of isomers **I1** and **I3** and a relatively low energy of **I4**.

The DFT calculations are able to reproduce the experimental X-ray structure of the [6,6]-methano derivative of $Y_3N@C_{80}$, a fulleroid with the addend located at an open [6,6] junction. Some of the most representative distances obtained from the X-ray characterization and from the computations are collated in Table 2. A very good agreement between the computed and observed values exists, the error being less than 0.03 Å for the selected distances. The formed bonds (fourth row in Table 2) with a C−C distance around 1.50 Å are shorter than in the case of pyrrolidine (1.55 Å) and Diels−Alder adduct (1.58 Å) formation.[29]

The calculations also show that for the low-energy orientational isomers (**I1**, **I3**, and **I4**) the [6,6] regioisomer is more stable than the [5,6] regioisomer in contrast with the behavior observed for the empty cage and for other high-energy orientations (see Table 1). For the empty C_{80} cage, the addition of a $C(CO_2CH_3)_2$ group at the [5,6] site is favorable by 6 kcal mol^{-1}. Previously, we reported that the encapsulation of a TNT stabilizes the [6,6] regioisomers more than the others and that this relative stability depends on the encapsulated metal. For the pyrrolidine addition, we found that for the Sc-based functionalized TMSs the [5,6] regioisomer is 12 kcal mol^{-1} more stable than the [6,6] one, but the energy difference between regioisomers is reduced to less than 2 kcal mol^{-1} when the metal is Y.[29]

Scheme 2. Schematic Representations of Open and Closed Functionalized $M_2@C_{80}$ Cages for Different Positions of the La_2 (Models **M1** and **M2**) and Sc_2 (Models **M3** and **M4**) Encapsulated Units

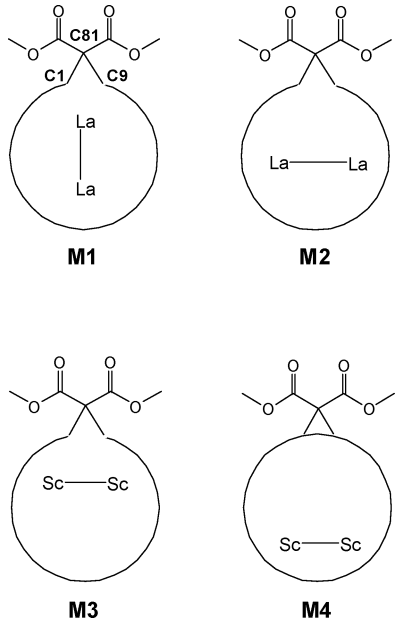

Will the Bingel−Hirsch Addition Produce Open or Closed Structures? Our computational studies show that the Bingel−Hirsch attack at a [6,6] bond of an empty C_{60} strongly weakens the functionalized bond as evidenced by the length change from 1.397 to 1.634 Å (DFT values). The same effect is observed for the I_h C_{80}; the functionalized [6,6] bond elongates from 1.428 to 1.625 Å. In both systems, we can consider that some residual interaction between carbons C1 and C9 (see Scheme 2 or Figure 3 for the numbering assignment) still remains after adduct formation. For $Y_3N@C_{80}$, only the [6,6] isomer **I5** shows a closed structure with a C1−C9 bond distance of 1.657 Å, but this isomer is very unstable (Table 2). For all of the other isomers the presence of the TNT unit inside the cage induces a lengthening of the C1−C9 distance up to ∼2.2 Å. We have performed some additional calculations on the model systems $M_2@C_{80}$ (M = Sc and La) to elucidate the main factors involved. For these compounds, a formal transfer of six electrons from the encapsulated unit to the carbon cage occurs as in TMS's. The isomers studied are schematically represented in Scheme 2.

For M = La, we obtained results equivalent to those of TMS's; the isomer in which one of the metal atoms is pointing to the external addend (**M1**) is much more stable (about 20 kcal mol^{-1}) than the isomer in which the two metals are far from the functionalized site (**M2**). This is an important fact; the direct interaction of C1 and C9 with the metal atom seems to strongly stabilize the compound. It must be pointed out that both **M1**

(39) Bader, R. F. W. *Atoms in Molecules. A Quantum Theory*; Oxford University Press: Oxford, U.K., 1994. Bader, R. F. W. *Chem. Rev.* **1991**, *91*, 893. Bader, R. F. W.; Hernandez-Trujillo, J.; Cortes-Guzman, F. *J. Comput. Chem.* **2007**, *28*, 4.
(40) Bo, C.; Sarasa, J. P.; Poblet, J. M. *J. Phys. Chem.* **1993**, *97*, 6362. Bo, C.; Costas, M.; Poblet, J. M. *J. Phys. Chem.* **1995**, *99*, 5914.

Table 3. Selected Distances (in Å) of the [6,6]-Methano Derivative of Different Fullerenes As Obtained from DFT Calculations (Labels of the C Atoms Refer to Scheme 2)

			$Y_3N@C_{80}$		$La_2@C_{80}$		$Sc_2@C_{80}$	
distances[a]	C_{60}	C_{80}	**I1**	**I5**	**M1**	**M2**	**M3**	**M4**
C81−C1[b]	1.506	1.514	1.503	1.505	1.500	1.490	1.490	1.512
C1···C9	1.634	1.625	2.277	1.657	2.206	2.192	2.184	1.646
charge transfer[c]			2.91	2.78	2.70	2.89	1.02	0.53

[a] See Scheme 2 for atom labeling. [b] Average value of the C81−C1 and C81−C9 distances. [c] Charge transfer (in e) from the encapsulated unit to the carbon cage obtained with the multipole derived charge method (MDC-q).

and **M2** are fulleroid-like structures. In **M2** the interaction of the metal with the carbon cage, and very probably the deformation of the cage induced by the TNT, favor the fulleroid structure.

Is it possible to retain some direct carbon−carbon interaction in the presence of an encapsulated guest? Let us discuss the $Sc_2@C_{80}$ system. For this model, we have computed the two forms, **M3** and **M4**, shown in Scheme 2. The Sc ion is smaller than the La ion, and the amount of charge transferred from the encapsulated unit to the carbon cage is less than for M = La, as shown in Table 3. When the Sc_2 unit is placed in the nonsubstituted hemisphere (**M4**), the structure of the cyclopropane unit consisting of C81−C1−C9 is similar to that of the empty C_{60} and C_{80}. However, this structure is not a stable form, and the guest prefers to be near the functionalized site. The form **M3** has a fulleroid-like structure that is about 10 kcal mol^{-1} more stable than the Sc_2-fullerene **M4**. Thus, it appears that it will be difficult to find circumstances in which the fullerene cage will remain intact in a Bingel−Hirsch adduct of an endohedral fullerene. Indeed, besides the TMS's **1** and **2**, Bingel−Hirsch cycloadducts of [$La@C_{82}$] have been suggested to have open type structures.[4]

Discussion and Conclusions

It is evident that the Bingel−Hirsch additions to EMFs follow paths that do not parallel those found for empty cages. As reported here, the crystallographic data of $Y_3N@C_{80}$−$C(CO_2CH_2Ph)_2$ show an open structure with metal ions located immediately adjacent to the site of addition, which resembles the structure of $La@C_{82}$−(Ad).[37] Unconventional products were also isolated when Akasaka and co-workers conducted the Bingel−Hirsch reaction with diethylbromomalonate and $La@C_{82}$.[4] Four EPR silent, singly bonded isomers of $La@C_{82}$−$CBr(COOC_2H_5)_2$, and one paramagnetic methano-adduct ($La@C_{82}$−$C(COOC_2H_5)_2$), whose anion ($[La@C_{82}−C(COOC_2H_5)_2]^-$) displayed ^{13}C NMR resonances similar to those of the anion of the [6,6]-open derivative of $La@C_{82}$, $La@C_{82}$−(Ad), were obtained with this reaction.

It is also apparent that the endohedral cluster plays a major role in directing the addition sites to EMFs. The crystal structures of $Y_3N@C_{80}$−$C(CO_2CH_2Ph)_2$ and $Y_3N@C_{80}$−$(CH_2)_2$-NEt show how two distinct types of cycloaddition reactions can occur for $Y_3N@C_{80}$ to produce very different products. In the Bingel−Hirsch adduct, $Y_3N@C_{80}$−$C(CO_2CH_2Ph)_2$, the [6,6] bond at the site of addition opens up and one of the yttrium atoms resides close to the addition site, while in the 1,3-dipolar cycloadduct, $Y_3N@C_{80}$−$(CH_2)_2$NEt, the Y_3N group is oriented so that two of the metal ions straddle the [5,6] site where the adduct is positioned.

On the basis of the capability of $Y_3N@C_{80}$ to undergo cycloaddition reactions, as demonstrated by the pyrrolidine products, and on its reactivity at [6,6] bonds, we propose that the bromomalonates add through the recognized Bingel−Hirsch cycloaddition mechanism. In such a case, the "closed" [6,6]-methano intermediate is expected to be energetically unstable, just like the [6,6]-pyrrolidino derivative,[6] but unlike this, the methano adduct is incapable of rearranging to the more stable [5,6]-adduct because it lacks the heteroatom needed to participate in the rearrangement mechanism, as we have previously proposed.[6,29] A possible (Scheme 3) thermally induced norcaradiene rearrangement might occur instead subsequent to the [6,6]-addition to result in cleavage of the cyclopropane ring and formation of an opening in the fullerene cage. We should note that we tried to compute the [6,6] closed adduct, but the optimization procedure always led to the open form. Even though we were unable to get a minimum in the potential surface corresponding to the proposed intermediate, we cannot dismiss its existence. Another possibility would be that both the cycloaddition and the formation of the fulleroid may occur concertedly. We are at present doing more accurate searches to find if in fact the "closed" methano participates as an intermediate in the formation of these monoadducts.

Scheme 3. Proposed Norcaradiene Rearrangement after the Bingel−Hirsch Cycloaddition To Form the $Y_3N@C_{80}$−$C(CO_2CH_2Ph)_2$ Fulleroid

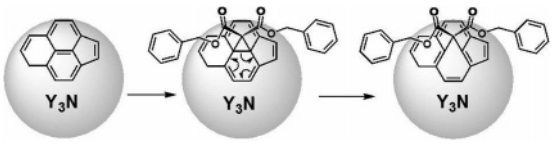

After a thorough experimental and theoretical characterization and analysis of the malonate monoadducts of $Y_3N@C_{80}$, we conclude that their stability must be attributed to the cage-open fulleroid structure, which allows for planarity of the trimetallic cluster inside the carbon cage and for the C_{80} cage to retain its sp^2 character. The introduction of this "handle" onto the $Y_3N@C_{80}$ structure will serve for the incorporation of this type of molecule into nanodevices without the risk of decomposition that is exhibited by the corresponding pyrrolidino addends.

Experimental Section

General. Commercially available materials were used as received unless otherwise specified. The $Y_3N@C_{80}$ (95%) was supplied by Luna Innovations (no traces of D_{5h} were detectable by HPLC) and used as received. ^1H and ^{13}C NMR spectra were recorded in a Bruker 500 MHz and referenced to TMS or the solvent used, as noted. UV/visible spectra were measured with a Shidmadzu UVPC-3101 spectrophotometer using a quartz cell with 1 cm path length. All electrochemical experiments, including CPE experiments, were performed using homemade cells as previously described, under high vacuum with $TBAPF_6$ as supporting electrolyte (0.05 M in *o*-dichlorobenzene).[41]

(41) Boulas, P. L.; Zuo, Y. H.; Echegoyen, L. *Chem. Commun.* **1996**, 1547−1548.

^{13}C-Labeled Dibenzylmalonate. ^{13}C-Labeled malonic acid (51.6 mg, 0.49 mmol), 4-dimethylaminopyridine (58.7 mg, 0.48 mmol), and 1-hydroxybenzotriazole (64.8 mg, 0.48 mmol) were stirred under argon in CH_2Cl_2 (30 mL). Following the addition of the ^{13}C-labeled benzyl alcohol (250 mg, 2.3 mmol), the mixture was cooled to 0−5 °C and the DIC (0.22 mL, 1.4 mmol) was added dropwise. The mixture was allowed to reach room temperature slowly and stirred for 4 days. The crude product was purified by column chromatography (SiO_2, $CHCl_3$) to produce 57.7 mg of the desired compound (41%, 0.20 mmol). ^{1}H NMR (500 MHz, $CDCl_3$): δ = 7.30−7.34 ppm (m, 10H), 5.16 ppm (d, J_{HC} = 148.3 Hz, 4H), 3.46 ppm (d, J_{HC} = 123.3 Hz, 2H). ^{13}C NMR (125 MHz, $CDCl_3$): δ = 166.44, 166.42, 165.96, 165.94, 135.39, 135.00, 128.57, 128.54, 128.39, 128.27, 128.24, 67.24, 41.55 ppm.

^{13}C-Labeled Bromodibenzylmalonate. ^{13}C-Labeled dibenzylmalonate (18.6 mg, 0.065 mmol) and CBr_4 (21.3 mg, 0.64 mmol) were dissolved in CH_2Cl_2 (5 mL) under argon. The solution was cooled to ca. 0−5 °C, and DBU (0.009 mL, 0.060 mmol) was injected. After 10 min, the solvent was evaporated, the residue was purified by preparative TLC, and 10.6 mg of the desired product was obtained (45%, 0.029 mmol). ^{1}H NMR (500 MHz, $CDCl_3$): δ = 7.29−7.35 ppm (m, 10H), 5.22 ppm (d, J_{HC} = 146.9 Hz, 4H), 4.91 ppm (d, J_{HC} = 160.0 Hz, 2H). ^{13}C NMR (125 MHz, $CDCl_3$): δ = 134.68, 128.68, 128.65, 128.34, 128.31, 68.75, 42.24 ppm.

$Y_3N@C_{80}$−$^{13}C(CO_2{}^{13}CH_2Ph)_2$ (2). The ^{13}C-labeled bromo-dibenzylmalonate (10.6 mg, 0.029 mmol) and DBU (0.0045 mL, 0.030 mmol) were dissolved in CH_3CN (4 mL). This solution was added dropwise to a solution of $Y_3N@C_{80}$ (5.07 mg, 0.0041 mmol) in *o*-dichlorobenzene (5 mL). After being stirred for 10 min under argon, the reaction mixture was purified by column chromatography (SiO_2, CS_2 followed by $CHCl_3$). No further purification was required (see HPLC trace of **2** in the Supporting Information). The unreacted $Y_3N@C_{80}$ (3.38 mg, 0.0027 mmol) was recovered from the CS_2 fraction (see Supporting Information), and 1.6 mg of the desired monoadduct was collected in the $CHCl_3$ fraction (76%, 0.0010 mmol). UV−vis (*o*-dichlorobenzene): λ_{max}, 401 nm (ϵ, 1.2 × 10^4), 547 nm (shoulder), 688−705 nm (ϵ, 1.1 × 10^3). ^{1}H NMR (500 MHz, $CDCl_3$): δ = 7.39−7.34 ppm (m, 10H), 5.28, 5.32, 5.58, 5.62 ppm (four dd, J_{HC} = 129.8, J_{HH} = 12 Hz, 4H). ^{13}C NMR (125 MHz, $CDCl_3$): δ = 69.54, 61.46 ppm. MALDI-MS (1,8,9-trihydroxyanthracene): *m*/*z* calcd for $C_{97}H_{14}NO_4Y_3$ 1522.81 $[M]^+$; found 1521.88.

X-ray Crystallography and Data Collection. Crystals of $Y_3N@C_{80}$−$C(CO_2CH_2Ph)_2{\cdot}0.5C_6H_6{\cdot}0.5CHCl_3$ were obtained by layering a chloroform solution of the adduct **2** in a 5 mm diameter tube with benzene. A second layer of acetone was placed over the benzene layer, and the sample was allowed to slowly evaporate. After 9 months, black crystals were harvested and used in the data collection. The crystals were removed from the glass tube in which they were grown together with a small amount of mother liquor and immediately coated with hydrocarbon oil on the microscope slide. A suitable crystal was mounted on a glass fiber with silicone grease and placed on the goniometer head in the cold dinitrogen stream from a CRYO Industries low-temperature apparatus at 90(2) K. The diffractometer was Bruker SMART Apex with an Apex II CCD and utilized Mo Kα radiation. Crystal data are given below. The structure was solved by direct methods and refined using all data (based on F^2) with the software of SHELXTL 5.1. A semiempirical method utilizing equivalents was employed to correct for absorption.[42] Hydrogen atoms were added geometrically and refined with a riding model.

Crystal Data for $Y_3N@C_{80}$−$C(CO_2CH_2Ph)_2{\cdot}0.5C_6H_6{\cdot}0.5CHCl_3$. $C_{100.5}H_{17.5}Cl_{1.5}NO_4Y_3$, fw, 1622.56; black needle; crystal size, 0.68 × 0.05 × 0.01 mm; orthorhombic; space group, $P2_12_12_1$; a = 11.2082(11) Å, b = 17.1248(16) Å, c = 27.882(3) Å, V = 5351.6(9) Å^3; λ(Mo Kα), 0.71073 Å; Z = 4, d_{calc} = 2.014 Mg/m^3; μ(Mo Kα) = 3.381 mm^{-1}; $2\theta_{max}$ = 50.5°; T, 90(2) K; 57 360 reflns collected, 9694 [R(int) = 0.1515] included in the refinement; 538 parameters, 3 restraints, wR_2 = 0.3006 for all data; conventional R_1 = 0.1013 computed for 6611 observed data with $I > 2\sigma(I)$.

Computational Methodology. The calculations were carried out by using DFT methodology with the ADF 2004 program.[45,46] The exchange-correlation functionals of Becke[45] and Perdew[46] were used. Relativistic corrections were included by means of the ZORA formalism. Triple-ζ + polarization basis sets were employed to describe the valence electrons of C, N, O, H, Sc, Y and La. All of the computed stationary points have closed-shell electronic structure. We have employed the computational model $Y_3N@C_{80}$−$C(CO_2CH_3)_2$.

Acknowledgment. This material was based on work supported by the National Science Foundation: ALB (CHE-0413857), CC, and LE (CHE-0509989 and LE while working at the Foundation). This material was also based upon work supported by Luna Innovations Incorporated and the Air Force Office of Scientific Research (AFOSR) under Contract No. FA9550-06-C-0010. A.R.-F. and J.M.P. thank the Spanish Ministry of Science and Technology [Project N. CTQ2005-06909-C02-01/BQU and the Ramón y Cajal Program (ARF)] and the DURSI of the Generalitat de Catalunya (2005SGR-00104) for economical support.

Supporting Information Available: Electrochemical, UV−visible, HPLC, and MALDI-MS characterization of **2** as well as crystallographic files (in CIF format); ^{1}H and ^{13}C NMR spectra of ^{13}C-labeled bis(benzyloxycarbonyl) bromomalonate; and Laplacian of the charge density distribution for the [6,6] isomer **I1** and pictures of the optimized geometries and bonding energies for the most stable [6,6] isomers (**I1**, **I3**, and **I4**). This material is available free of charge via the Internet at http://pubs.acs.org.

JA071733N

(42) Sheldrick, G. M. based on a method of R. H. Blessing, *SADABS 2.10*: *Acta Crystallogr., Sect. A* **1995**, *A51*, 33.
(43) *ADF 2004.01*, Department of Theoretical Chemistry, Vrije Universiteit, Amsterdam.
(44) Velde, G. T.; Bickelhaupt, F. M.; Baerends, E. J.; Guerra, C. F.; Van Gisbergen, S. J. A.; Snijders, G.; Ziegler, T. *J. Comput. Chem.* **2001**, *22*, 931−967.
(45) Becke, A. D. *Phys. Rev. A* **1988**, *38*, 3098−3100.
(46) Perdew, J. P. *Phys. Rev. B* **1986**, *33*, 8822−8824.